CHAPTER 3

SURFACE MODIFICATIONS OF NAFION MEMBRANE BY ARGON ION BEAM BOMBARDMENT AND PLASMA DEPOSITION COATING ON CARBON: MOLECULAR DYNAMICS AND MONTE CARLO STUDIES

3.1 Introduction

The basic structure of the PEMFC consists of layers of materials which having specific functions. Gases, H_2 and O_2 are diffused into system by gas diffusion layers or GDLs. The hydronium ion generated from anode of the electrolytic cell was transfer through Nafion, a polymer electrolyte fuel cell membrane with tetrafluorethylene sulfonic acid structure, to cathode. The membrane, catalyst layers (CLs) and two electrodes are assembled into a sandwich structure called membrane-electrode assembly (MEA). PEMFC performance depends on MEA efficiency thus it is the heart of the PEMFC [1]. Therefore, the development of fuel cell performance will be carried out by two approaches, membrane and catalyst improvement in this chapter.

3.1.1 Surface modifications simulation of electrolytic membrane

The research for fuel cell developments has been focused on the efficiency of polymer electrolytic membranes (PEM) in increasing electricity production efficiency and reducing the cost of PEM fuel cells. The direction of research is not only on the

development of alternative low-cost PEM [2-5], but also on the improvement of commercial PEM and Nafion, with the optimum chemical and physical properties.

The Nafion membrane has been modified by several approaches. The improvement of stabilized membranes at high temperatures was introduced to improve fuel cell durability and reliability [6,7]. To reduce costs of PEM fuel cells with low platinum catalyst loading and alternative catalysts have been developed [8-11]. Furthermore, the modification of the Nafion membrane surface, by experimental ion beam bombardment, results in an increase in the interface of the catalyst and electrode area. Cho *et al*. [12] and Prasanna *et al*. [13], studied Ar^+ ion beam bombardment on the surface of a Nafion membrane in order to increase the effective area of the catalyst/electrolyte interface [12], and to reduce the Pt loadings for the electrodes [13]. The roughness and hydrophobicity of the Nafion® 115 membrane surface were found to significantly increase, while the proton conductivity of the membrane was not affected by bombardment with Ar^+ ions (between 10^{15} and 10^{17} ions cm^{-2} at 1 keV). The membrane bombarded with an ion density dose of 10^{16} ions cm^{-2} at 1 keV exhibited the maximum power density. Beyond the optimum power and dose, the fuel cell performance decreased probably due to the loss of catalyst powers buried in the deep fissures on the membrane surface.

To simulate surface change from ion bombardment at a high energy range, Fekete *et al*. [14] modeled the effects of ion implantation into Nafion, using TRIM module of the SRIM program [14]. In this visual study, a selected series of the positive ions with energies of 20-320 keV, were used to bombard the target polymer.

They found that the ion energies of 100-200 keV can affect the outer 0.5-3 μm of the surface layer. The depth of the implanted ions in Nafion increases as the ion energies increased. Additionally, the collisions between ions and polymer moiety can alter the permeability of the Nafion membrane.

Atomistic simulation as MD simulation offers another choice for investigating the molecular changes of this phenomenon since MD simulation involves with the numerical solutions of the classical equations of motion. This computational method can help in the understanding of the properties of molecules, in terms of structure and the microscopic interactions [15,16]. Thus, it is necessary to study of the interactions between impacted ions and target polymers. In this study an attempt has been made to clarify the effects of ion implantation into the Nafion membrane on properties of bombarded Nafion. To study the theoretical account of the ion bombardment on the Nafion surface, at correlated low ion energy and ion doses reported by Cho *et al*. [12] and Prasanna *et al*. [13], MD simulations of Ar^+ bombardment on Nafion were investigated in the present study. A concrete explanation of the ion bombardment on modified Nafion will be considered here. The chemical and physical changes on the Nafion surface, resulting from the bombardment, will be compared with the experimental data in order to increase understanding into the effects of this treatment. The understanding of this microscopic phenomenon will help with the design of the fuel cell membranes using molecular level perception.

3.1.2 Plasma deposition simulation for alternative catalyst synthesis design

For alternative PEMFC catalyst development, the slow oxygen reduction reaction (ORR) kinetics on platinum (Pt) catalysts is among the most limiting factors in the energy conversion efficiency. Also, Pt has a high price [17,18]. Alternative materials are therefore highly sought for fuel cell applications. In fuel cell reduction process, one is production of water through a four-electron pathway, and the other is production of hydrogen peroxide through a two-electron pathway. The 4 and 2 electron reduction pathways were shown in equation (3.1) and (3.2) respectively [18].

$$O_2 + 4H^+ + 4e^- \rightarrow 2H_2O \quad (3.1)$$

$$O_2 + 2H^+ + 2e^- \rightarrow H_2O_2 \quad (3.2)$$

However, the harmfulness of anode material will become if the 2 electron pathway are occurred because acidity of H_2O_2 product. Also, Pt catalyzed cathode oxygen reduction is not a complete 4 electron reaction [19]. Therefore, the improvement of ORR catalyst should base on (i) high activity, (ii) low cost, and (iii) encouragement of 4 electron pathway. In order to reduce the cost of the fuel cell catalysts, two approaches are currently very active: exploration of non-noble metal catalysts, and reduction of the Pt loading. Non-noble metal catalyst, metal pyridine such as Fe-N/C, deposited Fe which has N as the ligand is one of employer [18-20]. In Fe-N/C catalytic sites, most possible structures of Fe-N/C are Fe-N_4/C and Fe-N_2/C as shown in Figure 3.1 [20].

In the reduction of Pt loading, plasma deposition of Pt dope on carbon support such as graphite was attempted [21].

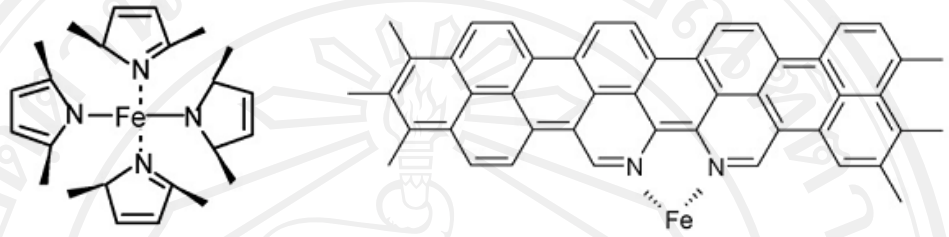

Fe-N_4/C Fe-N_2/C

Figure 3.1 Most possible structure of Fe-N/C [20]

In catalyst synthesis, not only thermal reaction of iron acetate with pure NH_3 and black carbon [19,20] but also nitrogen plasma deposition on carbon were introduced for improvement of ORR catalyst synthesis [22]. Temperature of plasma deposition (600 °C) was lower than thermal reaction (950 °C). The previous study of Hakoda *et al*. [22] found that their catalyst which was prepared by N_2 doped on heated carbon film gave high activity of ORR. Thus, the doping of nitrogen on carbon was leaded to interesting of Fe-N/C catalyst synthesis using nitrogen plasma deposition on carbon support. In this work, molecular simulations of nitrogen deposition coating on carbon surface model was employed to understand the molecular level properties and the information will be benefit for experimental design.

3.2 Methodology

3.2.1 Preparation of the Nafion model

The optimized structure of the Nafion side chain ($CF_3OCF_2CF(CF_3)OCF_2CF_2SO_3^-$; Figure 3.2) was taken from previous works [23,24]. The building unit was used to construct a Nafion model for MD simulation. The Nafion model consists of 1,024 side chains confined in a monoclinic MD box (Figure 3.2). The position of the side chains in the MD box were introduced based on the X-ray crystallographic data for trifluoromethanesulfonic monohydrate [25]. The total number of atoms in the simulation cell is 5,224 atoms. The energy structure of the model was minimized until the gradients were lower than 0.005 kcal/mol^{-1}. The optimized Nafion model was used for subsequent MD simulations. The NPT ensemble which number of particles, pressure and temperature were kept constant in the simulation was applied to the equilibration process of the system using Materials studio (MS) version 4.4 program package [26]. The COMPASS force field, a powerful force field that supports atomistic simulations of polymers, was used for all calculations [27,28].

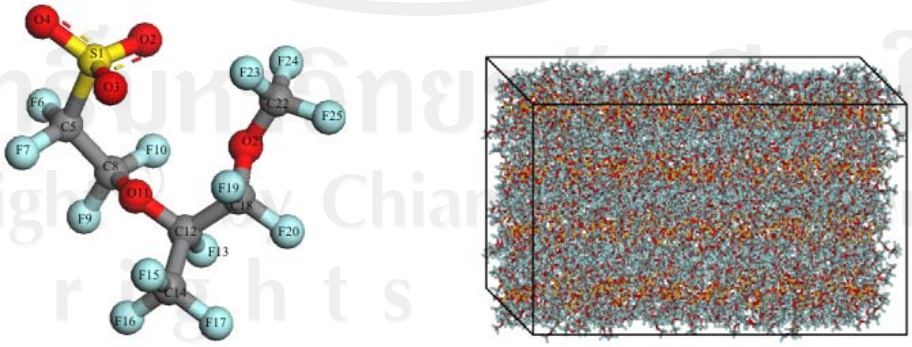

Figure 3.2 Structure of Nafion side chain (left) and MD box of Nafion model (right).

The MD time step was set at 1.0 fs, the pressure was set at 1.0 bar, and the target temperature was set at 298 K. The temperature of the whole system was gradually increased to the target temperature, in the first 60 ps, using Berendsen algorithm [29]. This was further performed at 298 K for 440 ps, and the last structure was kept for ion bombardment simulations. The dimensions of equilibrated Nafion model were 80x60x75 $Å^3$ with a density of 2.04 g cm^{-3} (Figure 3.2), corresponding to the value observed for Nafion®115 commercial data by the DuPont company.

3.2.2 MD simulations of ion bombardment on Nafion model

Two sets of MD simulations of the Ar^+ ions bombardment on the Nafion model were carried. These aimed to investigate the effect of the initial kinetic energy (KE) of the Ar^+ ions; and the effect of the Ar^+ ion dose on the bombarded Nafion. In the first set, six of MD simulations using canonical (NVT) ensemble with constant number of particles, volume, and temperature were performed at 353 K and each case study was repeated for three times to obtain a statistical average of the depths of implanted Ar^+ ions within the Nafion model. The initial KE of the Ar^+ ions was assigned at 0.5, 1.0, 1.5, 2.0, 2.5, and 3.0 keV, by varying the initial velocities of the Ar^+ ions, as computed from a typical kinetic energy function. The ion dose of $1x10^{14}$ ions cm^{-2} corresponded to 45 Ar^+ ions in the simulated system was used. These then generated Ar^+ ions beam were projected along the x-axis of the Nafion model, as shown in Figure 3.3. All ion bombardments were performed at normal incidence but at random positions of

the surface. In this study, non-periodic simulation was employed to investigate non-uniform ion bombardment scenario. In order to examine the effect of the ions dose in the bombardment on the Nafion, in correlation with experiments [12,13], the Ar^+ ions should be varied from $1x10^{14}$ to $1x10^{17}$ ions cm^{-2} with a KE of 1 keV. From the simulation, the bombardment using 45 Ar^+ shows strong inter-ion Ar ion-ion interaction during projection. In this study, Nafion model surface was generated with exposed area dimension of 60x75 $Å^2$. To avoid the edge effects of boundary potential and geometry in the simulation, the ion bombardment was limited to the central area away from the cell edge. The initial coordinates of Ar^+ in each simulation were randomly generated with their projection to the surface in a distance of 18-25 Å from the center. To impose the doses of 10^{14} - 10^{17} ions cm^{-2}, 45-4500 ions impacts should be simulated. However, from the simulation, the bombardment using 45 Ar^+ shows strong Ar ion-ion interaction during projection. Consequently, successive simulations were conducted to mimic the experimental study. For examples, to study of ion dose of $5x10^{14}$ ions cm^{-2}, five successive simulations were conducted with using 45 Ar^+ in each simulation. In each dose of the Ar^+ ions, the NVT-MD simulations were performed at 353 K, which is the working condition of a fuel cell. Each simulation was repeated three times to eliminate bias in the calculations. All bombardment simulations were performed with 1 fs time step, and, the simulation time for one ion impact trajectory was 1 ps.

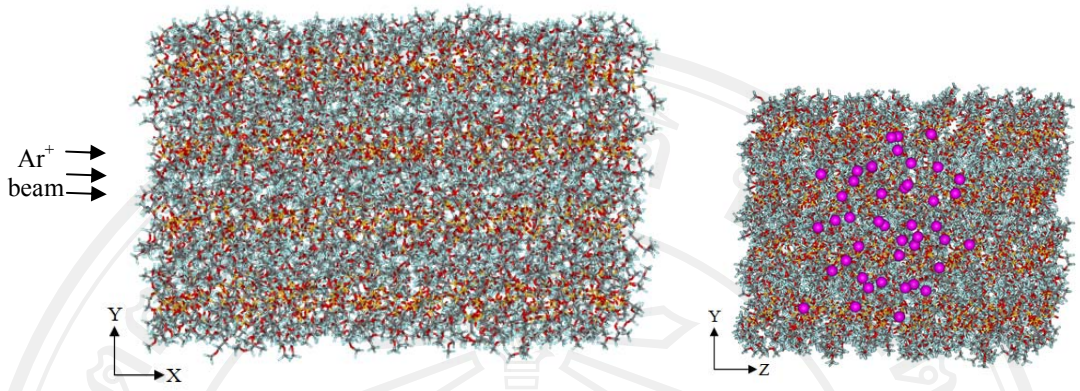

Figure 3.3 Model of Ar^+ ion bombardment on Nafion model viewed along XY plane and YZ plane.

3.2.3 Experimental study of the Ar^+ ion bombardment on Nafion

The investigations of Ar^+ ion bombardment on Nafion membranes were carried out in a sample preparation system of a photoemission experimental station of the beamline 4, at the Synchrotron Light Research Institute. Smaller pieces (0.5×0.5 cm^2) of Nafion®115 membranes were used for this work. The samples were chemically treated in 2 wt% H_2O_2 solution at 80°C for 60 minutes to remove organic impurities, then in de-ionized water at 80°C for 60 minutes, followed by sulfonation in 10 wt% H_2SO_4 at 80°C for 60 minutes to remove metallic impurities and to increase the sulfonic acid group, and finally in de-ionized water at 80°C for 60 minutes to remove the acid. The membranes were dried in a vacuum for over 2 days before introducing the samples into the sample preparation chamber, via the load-lock systems to prevent breaking UHV condition. It should be noted that the base pressure of the preparation

chamber was 2×10^{-10}Torr, however due to the high out gassing rate of the membranes, the vacuum pressure rose up to about 1×10^{-9}Torr.

A cold cathode ion sputter gun was used for ion bombardment. To produce Ar^+ ions, pure Ar gas was let in to the ion sputter gun, raising the vacuum pressure up to about 2×10^{-6}Torr. The energy of the ion was varied from 0.5 keV to3.0 keV, and the flux of the bombarding ions was measured using a Faraday cup located adjacent to the membrane sample. Quadrupole mass spectroscopy (QMS) was used for real-time determination of the amount of molecular species that were defragged by ion bombardment.

3.2.4 Model Preparation for deposition simulation

Molecular simulations of nitrogen plasma deposition on graphite sheet as carbon model were carried out by MC simulations. Carbon model was generated by repeating unit of graphite unit in 25x25x2 of X, Y and Z dimensions, with adding of vacuum above the 001 plane of surface for 200 Å as shown in Figure 3.4. In simulations study of nitrogen plasma coating on carbon model, all nitrogen species: N^+, N^-, N_2, and N_2^+ at $1x10^{15}$ particles.cm^{-2} were randomly deposited on the surface of carbon model at 353 K. The amount of nitrogen interact within 3.5 Å around carbon model was analyzed to describe the possibility of nitrogen doping.

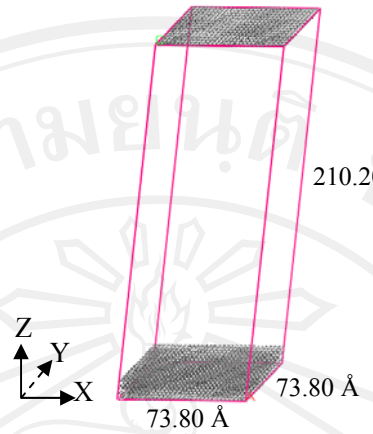

Figure 3.4 Carbon model

3.3 Results and discussion

3.3.1 Effects on energies/doses of Ar^+ ions on Nafion surface

From previous experiments [12,13], the effects of Ar^+ bombardment on Nafion membrane were analyzed through morphology, roughness and hydrophobicity of the surface. To investigate material characteristics at the atomistic level, the Nafion model after bombardment simulations was characterized in terms of damage profile and the implanted Ar^+ ions depth. The long-range modification of molecular arrangement in Nafion models with six different values of initial KE of Ar^+ bombarded on Nafion was considered as shown in Figure 3.5 Each condition introduces different profile depths to the x-axis of the Nafion model. The Ar^+ ions are randomly trapped in the Nafion structure. Although, the bond-breaking of Nafion fragments cannot be directly obtained from classical MD simulations, the dynamics of bombarded chains are distinctly different from the bulk region. The collisions result in a change of surface perceptual

structure which increases surface roughness and area. The damage cavity occurring within the Nafion model has an irregular shape with different sizes and depths along the x-axis of the Nafion.

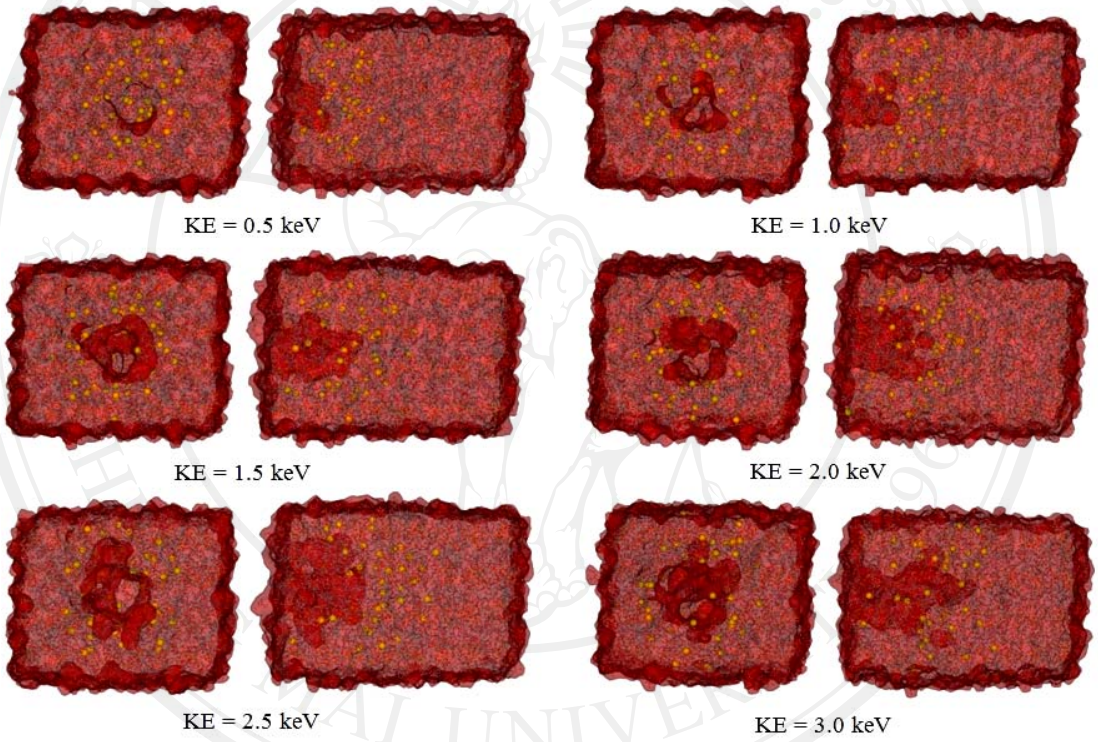

Figure 3.5 The damage cavity and implanted Ar^+ ions within Nafion model obtained from bombardment with six different values of initial KE of Ar^+ ions in YZ plane (left) and XY plane (right).

Penetration depths of Ar^+ in the Nafion model, with respect to initial KE values, are shown in Figure 3.6. The distances were measured frommaterial surface to the maximum Ar^+-trapped position. It is clear that the size and depth of the damage cavity, as well as

implantation depth of Ar^+ in the Nafion model, are in direct proportion to the initial KE value of the Ar^+ ions. These MD results correspond with the MC results observed by Fekete *et al*. [14] in which increasing the KE of bombarded ions increased the damage depth on the Nafion and the depth of implanted Ar^+ ions. This is reasonable since the collision of high KE particles on the target is more forceful than that of a low KE.

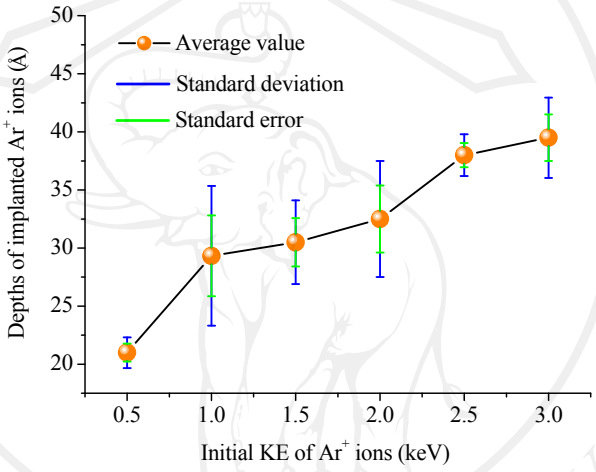

Figure 3.6 The depths of implanted Ar^+ ions along X-axis of Nafion model obtained from bombardment of Ar^+ ions with six different values of initial KE.

The morphology of the bombarded Nafion surface of each model, viewed along YZ plane, shows that surface area of the damage cavity was extended as the Ar^+ ions dose increased (Figure 3.7). The depth of damage cavity within the Nafion model, viewed along XY plane, shows that the damage cavity was also deeper into the Nafion model as of the Ar^+ ion dose increased. It is obvious that the depth of damage cavity was greater than that observed from the variation in the initial KE of Ar^+. These results may

have occurred as the Ar^+ ions dose density was increased and the number of times the Ar^+ ions beams directly struck the central area of Nafion model. This also increases the depth of the implanted Ar^+ ions in the Nafion model. The results obtained from this study are consistent with the roughness of the bombarded Nafion determined from surface images [12].

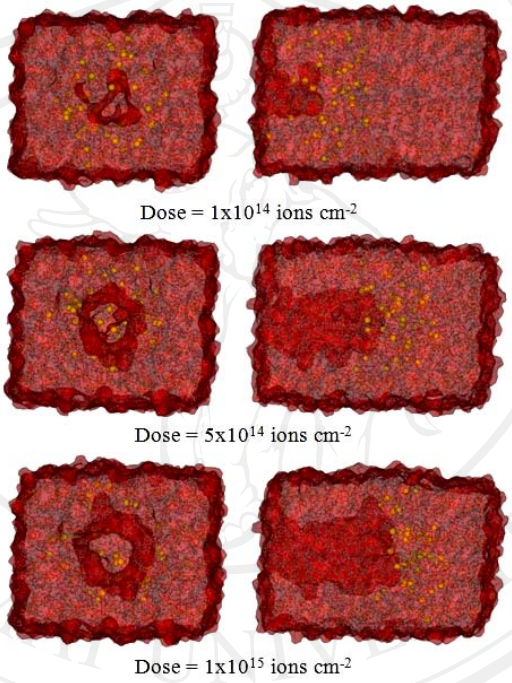

Figure 3.7 The damage cavity and implanted Ar^+ ions within Nafion model after bombardment with three different Ar^+ ions dose with energy of 1 keV in YZ plane (left) and XY plane (right).

3.3.2 Effect of Ar^+ ions bombardment on hydrophobicity of Nafion

Hydrophobicity of the bombarded Nafion was previously investigated by determining the water contact angle [12,13]. This is an important property of Nafion

since a hydrophobic surface can reduce the water content absorbed in the modified Nafion, while the proton conductivity of all membrane was almost constant [12]. In this study, the hydrophobicity of the bombarded Nafion was examined using SO_3^- sputtering from the Nafion surface. Since the polar SO_3^- group of the Nafion side chain can strongly bind with water molecules, it therefore adsorbs the water molecules within the Nafion.

Basically, the bond-breaking of a covalent bond can occurs if it is significantly elongate from the equilibrium distance [30].Therefore, the potentially breakable C-S bond of the Nafion was used as a criterion for analysis of the SO_3^- sputtering. In this work, the sputtering rate of SO_3^- fragment was calculated from sampling 10 side chains in each of bombarded and unbombarded Nafion model to analyze the fluctuation of C-S bond distances. In simulation time of 1 ps, the motion of Ar^+ reach a steady state implies all ion energy deposition on the surface. Structural data of the bombarded side chain located in the damage cavity, and unbombarded side chains were collected every 0.05 ps until reach into 1.00 ps for analysis (Table 1). Ten Nafion side chains of sampling were chosen from exposed part (10 angstrom from the surface) of the model. In other words, 10 chains are sampling of totally 128 side chains which is equal to 7.81 percentage of surface. The mean values of the C-S bond distances of unbombarded and bombarded side chains are 1.82 and 1.92 Å, respectively.

Table 3.1 Fluctuation of the C-S bonds in bombarded and unbombarded Nafion side chain.

C-S bond distance of unbombarded Nafion side chain (Å)											C-S bond distance of bombarded Nafion side chain (Å)									
Side chain no. / Time (ps)	1	2	3	4	5	6	7	8	9	10	1	2	3	4	5	6	7	8	9	10
0.00	1.80	2.04	2.01	1.75	2.01	1.78	1.61	1.68	1.72	1.91	1.67	2.03	1.64	1.79	1.83	1.65	1.69	1.67	2.08	2.17
0.05	1.84	1.68	1.56	1.86	1.69	1.67	1.77	1.85	1.65	1.63	1.60	1.47	1.75	1.60	2.20	1.63	1.69	1.52	1.63	2.03
0.10	1.91	2.03	2.12	2.01	2.02	1.82	1.66	1.60	1.90	1.87	2.66	1.87	1.05	2.13	1.87	2.41	1.48	1.87	1.82	1.83
0.15	1.59	2.06	1.92	1.99	2.00	1.76	1.58	1.80	1.67	1.67	1.85	2.02	1.78	2.63	2.78	1.51	2.53	2.09	2.87	2.44
0.20	1.92	1.82	1.74	2.07	1.93	2.06	1.76	1.55	1.79	1.66	1.84	1.39	2.04	2.27	2.36	2.51	2.35	1.98	1.53	2.40
0.25	1.65	1.72	1.43	1.93	1.96	2.04	1.59	1.83	1.96	1.91	1.30	1.38	1.93	2.46	2.21	2.25	2.38	2.59	1.62	2.01
0.30	1.99	2.08	1.69	2.05	1.75	1.92	1.61	1.65	1.84	1.80	2.17	2.15	1.65	1.92	1.90	1.67	2.48	2.47	2.20	2.38
0.35	1.87	1.91	2.11	1.90	1.75	1.74	1.59	1.68	1.85	1.76	1.78	2.15	2.18	1.75	2.75	2.08	2.27	2.54	2.32	2.42
0.40	1.81	1.79	1.79	1.92	1.84	1.65	1.64	1.61	2.06	1.84	1.63	2.32	1.88	2.19	2.89	1.80	2.01	2.09	1.59	2.63
0.45	1.82	1.77	1.78	2.11	1.87	1.68	1.63	1.65	1.88	1.90	1.58	1.65	1.45	2.27	2.14	2.34	1.77	1.95	2.25	2.26
0.50	1.87	1.76	1.66	1.99	1.82	1.73	2.05	1.59	2.03	1.90	1.71	1.75	1.94	1.77	1.85	1.90	1.67	2.52	1.99	2.26
0.55	1.77	1.77	2.09	2.06	1.84	1.84	1.67	1.62	2.01	1.98	2.04	1.46	2.13	2.05	2.45	2.32	2.03	1.69	2.07	1.86
0.60	1.95	1.64	1.92	2.01	1.87	1.71	1.79	1.56	2.07	1.87	1.49	1.65	1.52	1.98	2.00	1.61	1.57	1.48	2.26	1.88
0.65	1.73	1.67	1.81	2.08	1.98	1.73	1.74	1.56	1.94	1.86	1.69	1.54	2.24	1.92	2.18	1.73	1.70	1.89	1.67	1.78
0.70	1.87	1.60	1.82	2.01	1.84	1.68	1.80	1.58	1.94	1.87	1.76	1.77	1.68	1.96	1.48	2.03	1.45	2.28	1.70	1.90
0.75	1.79	1.64	1.74	2.03	1.86	1.60	1.71	1.59	2.01	1.89	1.88	1.39	2.00	1.78	2.06	1.98	1.67	2.02	2.00	1.94
0.80	2.04	1.52	1.92	2.06	1.76	1.72	1.80	1.60	1.95	1.86	1.79	1.65	1.90	1.62	1.84	2.01	1.56	1.79	1.98	1.82
0.85	1.80	1.67	1.84	2.01	1.92	1.88	1.86	1.59	2.05	1.87	1.70	1.82	2.02	1.71	2.22	2.06	1.58	1.87	2.06	1.88
0.90	1.83	1.66	1.73	2.07	1.94	1.79	1.72	1.61	2.07	1.80	1.75	1.44	1.98	1.37	2.22	1.82	1.56	1.83	2.09	1.84
0.95	2.02	1.62	1.68	1.98	1.91	1.72	1.83	1.70	2.07	1.92	1.75	1.62	2.31	2.08	2.65	2.06	1.48	1.89	1.97	1.70
1.00	1.90	1.64	1.79	2.11	1.98	1.69	1.83	1.61	2.00	1.83	1.66	1.73	1.99	1.58	2.14	2.03	1.65	1.84	1.90	2.06
Mean	1.85	1.77	1.82	2.00	1.88	1.77	1.72	1.64	1.93	1.84	1.78	1.73	1.86	1.94	2.19	1.97	1.84	1.99	1.98	2.07
Average of mean	1.82										1.92									
SD	0.11	0.17	0.18	0.09	0.09	0.12	0.12	0.09	0.13	0.09	0.27	0.28	0.29	0.31	0.36	0.28	0.36	0.32	0.31	0.27
Average of SD	0.12										0.30									
Maximum	2.04	2.08	2.12	2.11	2.02	2.06	2.05	1.85	2.07	1.98	2.66	2.32	2.31	2.63	2.89	2.51	2.53	2.59	2.87	2.63

The fluctuation of C-S bond distances was analyzed in term of standard deviation (SD). The SD value of 0.12 Å was found in unbombarded side chains while a higher value of 0.30 Å was found in bombarded side chains. The potentially broken C-S bond in the model was numbered in two alternative ways to ensure and validate the results. One was in terms of the percentage of the amount of C-S bond with an average distance higher than 2.22 Å (1.92 + 0.30 = 2.22). The other is the percentage of the amount of C-S bonds that have an SD value higher than 0.30 Å.

The results can imply that the Ar^+ ions bombardment on Nafion can cause increased hydrophobicity of Nafion as reported by Cho *et al*. [12] and Prasanna *et al*. [13]. The sputtering rate of SO_3^- fragments was examined from six MD simulations with a varied initial KE of Ar^+ ions ranging from 0.5-3.0 keV. These theoretical data were compared with experimental data derived from mass spectrometry. The sputtering rates of the SO_3^- fragment obtained from the experiment and computation are shown in Figure 3.8. The percentage of the amount of potentially broken C-S bonds after bombardment was derived from MD simulations and sputtering of SO_3^- fragments obtained from experimental data showed the same trends. The sputtering rate increased as the initial KE of Ar^+ ions increased. In addition, the calculated results confirm the thresholds at 2.0 keV as observed in experiment. Although the sputtering rate calculated from each MD result is higher than that observed from the experiment, the sputtering rate of SO_3^- computed from this work can still be used to describe the effect of initial KE of Ar^+ ions on the sputtering rate of SO_3^- fragments of Nafion.

a

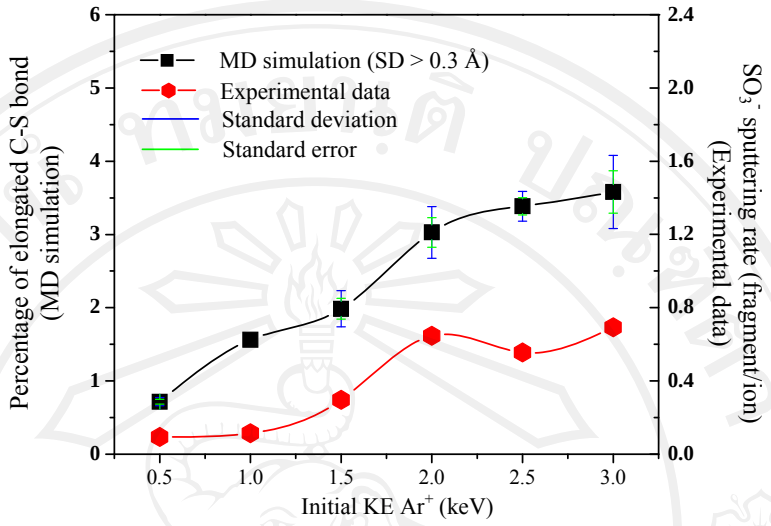

b

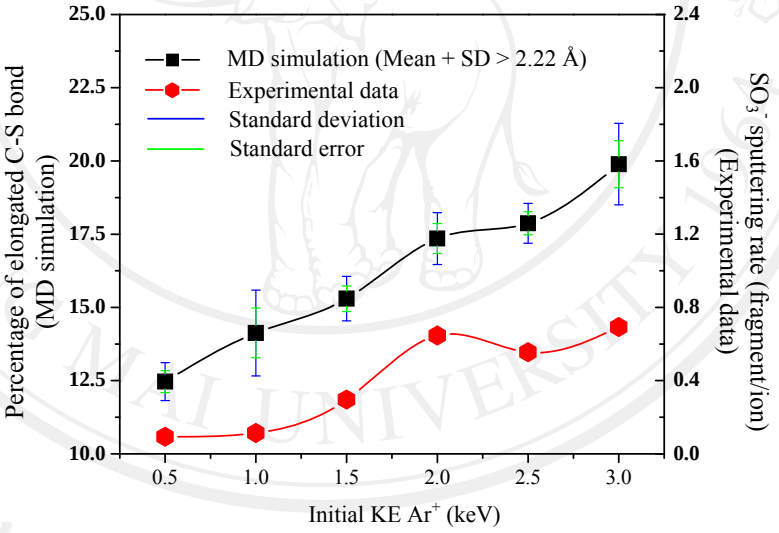

Figure 3.8 Comparison of potentially broken C-S bonds after bombardment and sulfonate fragment sputtering from experimental data. Amount of C-S bonds which have (a) SD value more than 0.30 Å and (b) distance average plus SD value more than 2.22 Å.

The different values of sputtering rates derived from simulations and the experiment explain that the percentage of the amount of potentially broken C-S bonds is computed from damage side chains in the specific damage zone. On the other hand, the experimental sputtering rate was measured from the amount of damage fragments that were sputtered out of a sample in both the overall bombarded and unbombarded regions. Moreover, in the simulations, all Ar^+ ions were forced to directly strike the Nafion model with the same initial KE for all Ar^+ ions; while the experimental Ar^+ ions generated from an ion source can move in all possible directions, depending on the repulsion forces, before they hit the specimen.

3.3.2 Distribution of nitrogen and iron on carbon model

The higher distribution of nitrogen plasmas than that iron was observed. The distribution of iron and nitrogen plasma within 3.5 Å around carbon model were shown in Figure 3.9. The iron cluster on carbon surface was found while the case of nitrogen was not. From this result, nitrogen plasma should be deposited at first step to activate surface for alternative FeN_x/C catalyst synthesis.

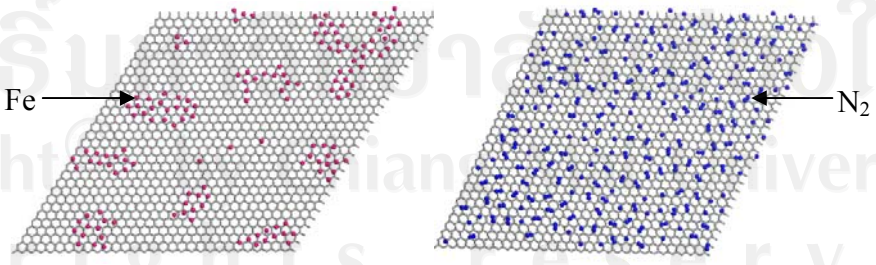

Figure 3.9 Distribution of iron (left) and nitrogen (right) around carbon within 3.5 Å

3.4 Conclusion

MD simulations and real-time determination of the amount of molecular species defragged under Ar^+ ion bombardment by quadrupole mass spectroscopy (QMS) were carried out to understand microscopic properties and this information can reveal the chemical and physical changes of Ar^+ initial energy and doses on Nafion modification. The variation of Ar^+ kinetic energies of 0.5, 1.0, 1.5, 2.0, 2.5, and 3.0 eV, at a dose of $1x10^{14}$ ions.cm^{-2}, was applied to the MD simulation to study the initial energy effect. While the variation of Ar^+ doses of $1x10^{14}$, $5x10^{14}$, and $1x10^{15}$ ions/cm^2 at 1.0 keV was designed to study the ion dose effect. From the MD simulation of low energy Ar^+ beam bombardment on the Nafion side chain cluster model, the Ar^+ bombardment on the Nafion surface can increase the surface area. The energy and dose of Ar^+ affect the surface roughness of the Nafion, and the Ar^+ energy potentially breaks the C-S bond, leading to SO_3^- sputtering decreasing the hydrophilicity of the bombarded Nafion. The percentage of potentially C-S bonds broken in the system for all Ar^+ energies are in agreement with the experimental SO_3^- sputtering measured by in-situ mass spectroscopy. As the higher initial kinetic energy from of Ar^+ was applied, percentage of elongated C-S bond analysed from MD trajectories increase but reach a local peak at 2.0 keV, then slightly decline down afterward confirming the thresholds at 2.0 keV as observed in experimental results. The simulation of nitrogen and iron plasma deposition on carbon model indicated that the distribution of nitrogen was higher than that of iron as cluster of iron after deposition was found. The information from this simulation is benefit for

experimental design; nitrogen plasma should be deposited at first step to activate the carbon surface for alternative FeN_x/C catalyst synthesis.

References

[1] Rabat, H.; Brault, P. *Fuel Cells* **2008**, *8*, 81-86.

[2] Smitha, B.; Sridhar, S.; Khan, A.A. *Journal of Membrane Science* **2005**, *259*, 10-26.

[3] Wang, Y.; Chen K. S.; Mishler, J.; Cho, S.C.; Adroher, X.C. *Applied Energy* **2011**, 88, 981-1007.

[4] Kreuer, K.D.; Fuchs, A.; Ise, M.; Spaeth, M.; Maier, J. *Electrochimica Acta* **1998**, *43*, 1281-1288.

[5] Herz, H.G.; Kreuer, K.D.; Maier, J.; Scharfenberger, G.; Schuster, M.F.H.; Meyer, W. H. *Electrochimica Acta* **2003**, *48*, 2165-2171.

[6] Starkweather, H.W. Jr. *Macromolecules* **1982**, *15*, 320-323.

[7] Corti, H.R.; Nores-Pondal, F.; Buera, M.P. *Journal of Power Sources* **2006**, *161*, 799-805.

[8] Bezerra, C.W.B.; Zhang, L.; Lee, K.; Liu, H.; Marques, A.L.B.; Marques, E.; Wang, H.; Zhang, J. *Electrochimica Acta*, **2008**, *53*, 4937-4951.

[9] Zhang, L.; Zhang, J.; Wilkinson, D.P.; Wang, H. *Journal of Power Sources* **2006**, *156*, 171-182.

[10] Charreteur, S.; Ruggeri, S.; Jaouen, F.; Dodelet, J-P. *Electrochimica Acta* **2008**, *53*, 2925-2938.

[11] Charreteur, F.; Jaouen, F.; Ruggeri, S.; Dodelet, J-P. *Electrochimica Acta* **2008**, *53*, 6881-6889.

[12] Cho, S.A.; Cho, E.A.; Oh, I.H.; Kim, H.-J.; Ha, H.Y.; Hong, S.-A.; Ju, J.B. *Journal of Power Sources* **2006,** *155*, 286-290.

[13] Prasanna, M.; Cho, E.A.; Kim, H.-J.; Lim, T.-H.; Oh, I.-H.; Hong, S. *Journal of Power Sources* 2006, 160, 90-96.

[14] Fekete, Z.A.; Wilusz, E.; Karasz, F.E. J*ournal of Polymer Science: Part B: Polymer Physics* **2004**, *42*, 1343-1350.

[15] Allen, M.P.; Tildesley, D.J. "Computer Simulation of Liquids" Clarendon Press, Oxford, **1987**.

[16] Leach, A. "Molecular Modelling: Principles and Applications" 2nd ed.; Prentice Hall, **2001**.

[17] Wang, B. *Journal of Power Sources* **2005**, *152*, 1–15.

[18] Bezerra, C.W.B.; Zhang, L.; Lee, K.; Liu, H.; Marques, A.L.B.; Marques, E.; Wang, H.; Zhang, J. *Electrochimica Acta*, **2008**, *53*, 4937-4951.

[19] Charreteur, S.; Ruggeri, S.; Jaouen, F.; Dodelet, J-P. *Electrochimica Acta* **2008**, *53*, 2925–2938.

[20] Charreteur, F.; Jaouen, F.; Ruggeri, S.; Dodelet, J-P. *Electrochimica Acta* **2008**, *53*, 6881–6889.

[21] Honma, I.; Hirakawa, S.; Yamada, K.; Bae, J.M. *Solid State Ionics* **1999**, *118*, 29–36.

[22] Hakodaa, T.; Yamamotoa, S.; Kawaguchib, K.; Yamakia, T.; Kobayashic, T.; Yoshikawaa, M. *Applied Surface Science* **2010**, *257*, 1556–1561

[23] Yana, J.; Lee, V.S.; Nimmanpipug, P.; Dokmaisrijan, S.; Aukkaravittayapun, S.; Vilaithong, T. *Journal of Solid Mechanics and Materials Engineering* **2007**, *1*, 556-563.

[24] Yana, J.; Nimmanpipug, .; Chirachanchai, S.; Gosalawit, R.; Dokmaisrijan, S.; Vannarat, S.; Vilaithong, T.; Lee, V.S. *Polymer* **2010**, *51*, 4632-4638.

[25] Spencer, J.B.; Lundgren, J.O.; *Acta Crystallographica Section B: Structural Science* **1973**, *29*, 1923-1928.

[26] Materials Studio, Accelrys Software Inc., San Diego, CA, **2007**.

[27] Martin, M.G. Fluid Phase Equilibria **2006**, *248*, 50-55.

[28] Sun, H. *Journal of Physical Chemistry B* **1998**, *102*, 7338-7364.

[29] Berendsen, H.J.C.; Postma, J.P.M.; van Gunsteren, W.F.; DiNola, A.; Haak, J.R. *Journal of Compational Physics* **1984**, *81*, 3684-3690.

[30] Ngaojampa, C.; Nimmanpipug, P.; Yu, L.; Anuntalabhochai, S.; Lee, V.S. *Journal of Molecular Graphics and Modelling* **2010**, *28*, 533-539.